IMPERIAL COLLEGE LONDON

Department of Earth Science and Engineering

Centre for Petroleum Studies

Packing characteristics of different shaped proppants for use with hydrofracing
– A numerical investigation using 3D FEMDEM

By

Chern Zherng Low

A report submitted in partial fulfillment of the requirements for the MSc and/or the DIC in Petroleum Engineering.

September 2011

DECLARATION OF OWN WORK

I declare that this thesis "*Packing characteristics of different shaped proppants for use with hydrofracing – A numerical investigation using 3D FEMDEM*" is entirely my own work and that where any material could be construed as the work of others, it is fully cited and referenced, and/or with appropriate acknowledgement given.

Signature: …………………………………………………..

Name of student: Chern Zherng Low

Names of supervisors: Dr. John-Paul Latham, Dr. Jiansheng Xiang, Prof. Alain Gringarten

ACKNOWLEDGEMENTS

List of Figures

List of Tables

Table of Contents

Packing characteristics of different shaped proppants for use with hydrofracing – A numerical investigation using 3D FEMDEM

Chern Zherng Low

Jiansheng Xiang, John-Paul Latham, Alain Gringarten

Abstract

This paper describes a Combined Finite-Element Discrete Element Method (FEMDEM) approach to modelling the packing porosity of cylindrical proppants at 10:1 scale settling under gravity. These investigations were performed at a 10:1 scale because of industry interest in particle scale simulations. The aim of this work is to first, quantify the effects of aspect ratio, and friction coefficient on the packing porosity of cylindrical proppants, and secondly, to investigate the effect of aspect ratio on the stress distribution within cylindrical proppants. Such simulations provide insight on the optimal cylinder aspect ratio which packs to higher porosity, and consequently, higher permeability, while withstanding a chosen fracture closure stress of 25 MPa.

These were performed using a 3D FEMDEM code ,Y3D, included in an open source suite of geoscience simulation tools (VGeST) resulting from a 5 year collaborative research project between Imperial College London (Latham) and Queen Mary, University of London (Munjiza). FEMDEM has advantages over the discrete-element method (DEM) based on spheres and superquadrics, because it allows complex geometries to be introduced easily. In addition, the contact algorithms implemented also make it an efficient method for simulating large numbers of interacting bodies in a single model.

Our simulations results of packing porosity of different aspect ratio cylinders with 3D FEMDEM showed a good agreement with experiments and simulations of cylinder packing found in literature. The packing structures of cylinders near the wall are also realistically reproduced in our simulations. Unfortunately, because we attempted to simulate as closely to particle scale as we thought was possible, the friction and stress loading simulations could not be concluded in the timeframe of our research. Additional simulations performed at 1000:1 scale showed that the total computational time was reduced up to 8 fold when compared to 10:1 scale simulations.

We will briefly present the theory behind the contact algorithms and implementation of deformability in FEMDEM. The mesh generation workflow is explained, and we detail the simulation setups and justify the choices of key simulation parameters because the FEM component captures the deformability of each discretely interacting particle. It can also capture internal stresses which are vital for assessing the proppant survivability under applied stresses. Key findings are presented and discussed along with recommendations for future work. Our simulation results of cylinder aspect ratio show lowest porosity of 40% for equilateral cylinders, and increases to 47% as aspect ratio increases up to 4.0.

1   Introduction

Since the 1950s, hydraulic fracturing has been used to stimulate wells of reservoirs comprised of tight formation rock where it would otherwise be uneconomic to develop. A typical hydraulic fracturing job consists of pumping hydraulic fracturing fluid with a suspension of proppants in varying concentrations determined in the design stage, into the reservoir borehole. As hydraulic fracturing pressure increases, hydrofrac fluid leaks-off into the reservoir, leaving the proppants lodged in newly created fractures. When pressure equilibriates and reduces below reservoir pressure, the fractures close on these proppants, and they remain propped open. The success of a stimulation job can be gauged by the increase in hydrocarbon production afterwards due to improved fracture conductivity (SPE 143426).

Fracture conductivity depends on the permeability in the fracture (Prats 1961), and this is strongly related to the porosity by Carmen-Kozeny's (Kozeny 1927, Carman 1937) and Ergun's correlations (Ergun 1952). In field tests, hydrofracing proppants that form high porosity packs in laboratories have been known to increase hydrocarbon production more than dense packing proppants (SPE 135360). This could be due to improved pore interconnectivity from enlarged pore throats found in high porosity proppant packs. Other favourable hydraulic fracturing behaviours are also observed in high porosity proppant packs, such as increased proppant flowback resistance (less proppant is required), increased cleanup of hydraulic fracturing fluids (less clogging), and alignment parallel to the flow (decreased pressure loss). These benefits associated with high porosity packs interest the industry, and have prompted more research into the packing behavior of cylindrical proppants.

The main consequences of changing particle geometry are the impact on the packing behavior, and the failure modes of the subsequent packed bed (SPE 135360). The packing behaviour of spheres is very well studied, and its porosity is reported to range from 36% to 42%. Packing behavior of cylinders is more complex as they show orientational freedom, and is reflected in the wider range of porosity (24% to 45%) documented in literature for equilateral cylinder packings (Wenli Zhang 2006). While the quantitative analysis of cylinder packing porosity in literature is limited at the particle scale because of the difficulty in simulating non-spherical particles using traditional techniques, there is even less evidence of stress loading experiments on cylindrical particles. The stress loading of cylinder shaped proppant has only been investigated by proppant manufacturers performing tests according to API Standard Recommended Practice 19 guidelines (API RP 19C 2008), which report breakage percentage for a specified test stress. There is no other method of evaluating new proppant geometries without first producing samples and then testing them.

In this paper, we will introduce a framework to perform preliminary investigations which may provide some answers by employing 2 versions of the **3D FEMDEM** code. The first, is called **Y3D_D** (D for deformable), and it evaluates the stresses and deformations in a particle. The other version is **Y3D_R** (R for rigid), and it assumes a body is rigid and skips the deformation calculations. This rigid version runs significantly faster and is used for our packing porosity investigations since very little deformation is expected for gravity deposited particles at 10:1 scale. It is worth noting that small particles will increase the computational time required. We chose this scale to provide data as close to particle scale as possible numerically within our investigation timeframe. Likewise, the deformable version, Y3D_D, is used for our stress loading simulations at 10:1 scale. High aspect ratio cylinders under stress will experience additional 3-point-bending modes that will induce both tensile and compressive stresses on a particle which will significantly reduce the strength of ceramic cylinders.

2   Background

2.1   Cylinder packing experiments

Experimental investigations on the packing behaviour of cylinders are less commonly performed than spheres, even though they are also of great importance in understanding flow through columnar beds, and catalytic reaction bed applications.

Roblee et al. (1958) packed cylinders in a column and filled the void spaces with wax. Radial shells of the solid cylinder were removed carefully, and weighed to determine the porosity. The shells were analysed using radial density functions, and oscillations can be observed up to 3 diameters from the wall. These oscillations exhibited sinusoidal damping behavior which stabilises at the centre of the pack. They reported a porosity of 25% for equilateral cylinders. This porosity is much lower than documented anywhere else, and could be due to wax not fully filling void spaces before solidifying. Dixon (1988) carried out cylinder packing experiments which were later used to develop an empirical correlation between porosity as a function of tube-to-particle diameter ratio. He reported a porosity of 36% for loose packing of equilateral cylinders. Nardin et al. (1985) created loose and dense packings of polypropylene cylinders for a range of aspect ratios up to long fibres. They noted that the porosity increases with aspect ratio, and reported a porosity of 46.2% for loose packings of equilateral cylinders.

Foumeny and Roshani (1991) packed steel cylinders of a range of aspect ratios (0.5 to 3) into cylindrical containers with light vibration to encourage random packings. The porosity of the packing was determined using a water displacement method which was also employed by Sharma et al. (2001) in their flow experiments. A porosity correlation based on tube-to-diameter ratio was introduced for a range of cylinders with aspect ratios of 0.5 to 3. Benyahia (1996) packed lead equilateral cylinders into a cylindrical mould and filled the void spaces in the packing with dyed resin to provide colour contrast. The solid column was then sliced at 1mm intervals and the packing structure was processed using an image analysis program. They reported that the mean packing voidage with equilateral cylinders is lower than non-equilateral cylinders and spheres for comparable container-to-particle ratios. Wall and end effects extend about 3 diameters from the container walls. For aspect ratios of 0.5, the end effects are eliminated before 2 diameters from wall. Zou and Yu (1996) performed experiments on loose and dense packing of cylinders and disks using different column diameters and correlated them by introducing a concept of equivalent packing diameter. Equivalent packing diameter is defined as the diameter of an equivalent sphere containing the same volume as the non-spherical particle. The correlation is based on particle sphericity ψ, which is defined as the ratio of the surface area of a sphere with the same volume as the particle to the surface area of the particle. From this, the porosity of equilateral cylinders is calculated to be 40.4%.

Montillet and Le Coq (2001) performed packing experiments on PVC cylinders with aspect ratio 5.29, and focused their analysis on characterizing the wall and end effects. The packings were poured and compacted with a piston, void spaces were filled with dyed resin for image analysis. They observed that bottom end effects can be seen as longitudinal variations in porosity, and top end effects result in high mean porosity within 2 to 3 equivalent sphere diameters. Lumay and Vandewalle (2004) investigated the tapped packing porosity of cylinders of different length to container diameter ratios. Loose packs were prepared by pouring solid pasta cylinders into a glass tube and then tapping is introduced using a computer controlled

electromagnetic hammer. They found that when the cylinder length equals the container diameter, the packing porosity of equilateral cylinders ranges between 42 to 50%. This range is among the highest quoted in literature, and is due to some cylinders with horizontal orientations causing jams in the container. They also observed that as cylinder length to container diameter ratio increases, more cylinders align in the vertical orientation and form denser packings as a result. This behavior was also shared by Villarruel et al. (2000) in a similar setup involving vibrated packs of cylinders of aspect ratio 3.89 in a vertical tube (tube diameter to cylinder length ratio = 2.71). Benyahia and O'Neil (2005) introduced an empirical correlation for cylinders with aspect ratios 0.76 to 1.78. A water displacement technique was used in their experiments to measure the packing voidage of cylinders. The porosity of equilateral cylinders packings in a container with tube-to-particle diameter ratio of 15 is 38.8%.

2.2   Numerical simulation of packing

There are 2 main types of numerical simulation approaches to particle packing: geometric approaches, and mechanical approaches. Examples of geometric approaches are sequential deposition, Monte Carlo, and mechanical contraction algorithms. These algorithms only take into account the geometry of the particles, and the only constraint enforced is that no overlaps are allowed. Geometric approaches ignore friction, contact forces, and stress mechanics, and are often very computationally efficient. Realistic sphere packs have been created using these approaches with good agreement with packing experiments. Cylinder packing simulations are even rarer than experimental investigations mainly because geometric packing algorithms used to generate sphere packings cannot be adapted to cylinder packings.

The earliest simulation of cylinder packings was done by Vold (1959, 1960, 1963) to replicate sedimentation behavior of colloidal particles in suspension. He employed a geometric numerical model to deposit randomly oriented cylinders (aspect ratios of 1 to 18) from random locations above a rectangular container. These particles were allowed to drop in a vertical trajectory until it contacts a previously deposited particle and its motion is frozen. He observed that his simulations produced packing porosities up to 2.5 times larger than his experiments. Coelho et al. (1997) simulated ellipsoids, parallelepipeds, and cylinders with varying aspect ratios (1 to 10) using a sequential deposition (SD) algorithm. He reported that equilateral cylinders packed to a porosity of 44.8%, which would represent the upper bound porosity for equilateral cylinder packings. This characteristic larger packing porosity is also seen in other implementations of sequential deposition packing algorithm simulations by Sherwood (1997) and Nandakumar (1999).

Visscher and Bolsterli (1972) used a different geometric method called the Monte Carlo packing algorithm to generate random sphere packings. This algorithm randomly fills a space with the particle and removes particles when there is an overlap. They reported an average porosity of 40% at the central bulk of the sphere packs. Wenli Zhang (2006) generated packings of non-spherical particle commonly found in catalyst beds, using commercial Monte Carlo packing algorithm called DigiPac. Their findings suggest that while it can predict trends in packing porosity of different geometries, it fails to replicate ordering patterns observed in experimental results. Stoyan et al. (1998, 2006), Williams and Philipse (2003), and Wouterse et al. (2007) simulated dense packings of spheres, spheroids (Figure 1), and spherocylinders using a mechanical contraction packing algorithm. Particles are placed randomly within a defined volumetric domain, starting from the extremities. At each timestep, the domain contracts and more particles are placed without allowing overlaps.

Figure 1 – Geometric random packing of 4000 oblate spheroids. (Stoyan 2006)

While there have been attempts to create cylinder packs with geometrical approaches, the general conclusion is that this approach is inadequate for creating realistic cylinder packs. The orientational freedom that cylinder particles exhibit creates complex packing patterns not observed in sphere packings because of wall contact forces, wall and particle friction, particle orientation, jamming, and volume exclusion effects. This introduces the need for mechanical approaches which incorporate mass, contact, and friction mechanics.

The Discrete Element Method (DEM) is a mechanical approach proposed by Cundall and Strack (1979) which has been extensively used for simulating large numbers of particles in granular, particle, and rock mechanics problems. DEM incorporates contact force interactions, friction, and rotational degree-of-freedom. Each particle is treated as a seperate entity, and their velocity, rotation, and position is calculated and updated after every timestep. The velocity and rotation mechanics are desribed by Newtonion laws and evaluated by integration over the timestep. The contact force model employed varies depending on DEM implementation, but energy and momentum must be conserved to maintain numerical stability. The main drawback of DEM codes is that complex geometries cannot be introduced easily. Most DEM codes based on superquartics introduce slight bumps due to the reliance on clustering spheres and reduce simulation accuracy. In the next section, we will introduce the combined finite-discrete element method (FEMDEM) theory which is the framework used in our investigations.

3   Combined FEMDEM Theory

Munjiza (1990) introduced a combined finite-discrete element method (FEMDEM) which bridged discrete-element modeling (DEM) with finite-element modeling (FEM). Each discrete element is discretised into finite elements and the stress within each finite-element is calculated. This allows deformation, fracture and fragmentation behaviors to be captured. Prior to 2005, 3D FEMDEM codes were mainly based on linear 4-node tetrahedral finite elements and have 2 drawbacks. Firstly, volumetric locking problems in discrete elements associated with incompressible solids can result in inaccurate simulations. Secondly, deformation was not addressed properly and a body was treated as a rigid entity with only surface finite element meshing.

A new 3D FEMDEM code, Y3D, has been developed by Dr J Xiang under direction of Prof. Munjiza as part of VGW virtual geoscience workbench tools, to address the limitations associated with traditional 4-node tetrahedron based FEMDEM codes. This code implements an efficient quadratic 10-node tetrahedron element together with an F-bar approach (Neto 2005) to overcome locking, and stress propagation wave issues. The F-bar approach splits the deformation gradients into separate deviatoric and volumetric terms, and averages the incompressibility constraint throughout the element instead of at a point which avoids locking due to constant strains. Illustration of the stress propagation in collisions mechanics modeled with Y3D was given in (Xiang et al. 2009) by simulating a concrete cross shaped structure dropped onto a giant anvil. The Cauchy stress propagation waves can be observed in the Figure 2. An earlier validation of the FEMDEM method based on results for packing characteristics of real particle shapes was reported by Latham and Munjiza (2004) by comparing cube-packing experiments with numerical, and they concluded that the results were qualitatively in good agreement (Figure 3). However, this earlier version of the FEMDEM code assumes rigid particles (no deformation).
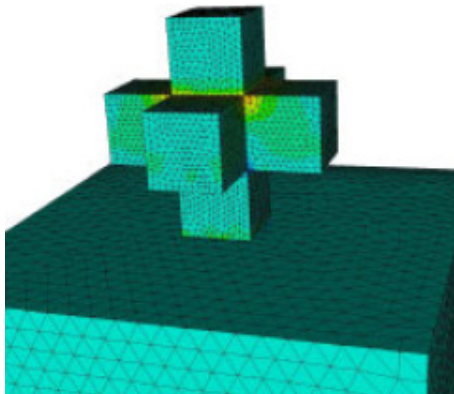
Figure 2 – Cauchy stress Y3D simulation of concrete cross-shaped structure dropped onto a giant anvil. (Xiang et al. 2009)

Figure 3 – Comparison of cube packing structures from Y3D simulation and experimental setup. (Latham and Munjiza 2004)

A brief overview on the key modules of FEMDEM implementation such as the contact detection, contact interaction, and deformability theory is presented here. For a more in-depth explanation of the theory, refer to (Munjiza 2004)

3.1   Contact detection

Contact detection and contact interaction algorithms built into FEMDEM allow transient problems with large numbers of interacting deformable bodies to be modeled efficiently. At each time step, the contact algorithms are executed. The main function of Munjiza's NBS (no binary search) contact detection algorithm is to reduce the total computational time by detecting discrete elements which are close by and ignoring those which will never contact in that timestep. This is accomplished by first dividing space into identical cells large enough to contain the largest discrete element in the system, and then individually mapping discrete elements to a cell which can only contain one unique discrete element. Only discrete elements from neighbouring cells can touch each other, so those which will not contact are ignored. (Munjiza 2004)

There are numerous contact detection algorithms available, but the optimal algorithm depends largely on the type of problem solved. Munjiza and Andrews (1998) NBS linear contact algorithm uses less CPU resources than binary search algorithms in problems with a large number of discrete elements because the detection time for a discrete element is constant, unlike binary search algorithms. This linear increase in total detection time with the number of discrete elements modeled makes it well suited for simulating packing density of particles.

3.2   Contact interaction

Once couples of contacting discrete elements are detected, a contact interaction algorithm then evaluates the contact forces for these coupled discrete elements. The way an algorithm handles contact interaction defines the constituent behavior of the system because of the large numbers of separate bodies (Munjiza 2004). Therefore, it is critical that the contact kinematics is described realistically by algorithms used. A contact interaction algorithm based on the penalty function method is implemented in this code, and in its classical form assumes that two bodies in contact (a contactor and target body, Figure 4) will penetrate each other (Munjiza and Andrews 2000). The resultant contact force is directly related to the amount of overlap between the 2 bodies.

There are two approaches to evaluating the contact force; a concentrated or a distributed contact force approach. A distributed contact force approach which discretises individual discrete elements into finite elements is used in this FEMDEM code. It is easier to implement than a concentrated contact force approach, and also preserves energy balance regardless of the number and geometry of the discrete elements in contact. This yields realistic contact force distributions and overcomes the numerical distortion of force distributions associated with concentrated contact force approach, so it is suitable for instantaneous fracture simulations.

When a contactor penetrates any elemental volume dV of the target discrete element, the total resultant infinitesimal contact force is given by:

$$d\boldsymbol{f} = [grad\ \emptyset_c(P_c) - grad\ \emptyset_t(P_t)]dV \tag{1}$$

where $d\boldsymbol{f}$ is the infinitesimal contact force due to overlapped volume dV, $\emptyset_c$ is the potential of the contactor, and $\emptyset_t$ is the potential of the target.

By integrating over the overlap volume, the total contact force exerted by the target onto the contactor can be written as an integral over the surface S of the overlapping volume, like so:

$$\boldsymbol{f} = \int_{S_{\beta_c \cap \beta_t}} \mathbf{n}(\varphi_c - \varphi_t)\ dS \tag{2}$$

where $\mathbf{n}$ is the outward unit normal to the surface of the overlapping volume.

The potentials φ_c and φ_t are obtained by the summation of potentials associated with its individual finite elements.

$$\varphi_c = \varphi_{c_1} + \varphi_{c_2} \dots + \varphi_{c_i} + \varphi_{c_n} \tag{3}$$
$$\varphi_t = \varphi_{t_1} + \varphi_{t_2} \dots + \varphi_{t_i} + \varphi_{t_n} \tag{4}$$

(Munjiza 2004) demonstrated that the contact force between overlapping discrete elements is calculated by summation over the edges of corresponding finite elements that overlap.

$$\boldsymbol{f_c} = \sum_{i=1}^{n} \sum_{=1}^{m} \int_{\Gamma_{\beta_{c_i} \cap \beta_{t_j}}} \mathbf{n}_{\beta_{c_i} \cap \beta_{t_j}} \left(\varphi_{c_i} - \varphi_{t_j}\right) d\Gamma \tag{5}$$

where, m and n are the total number of finite elements which the contactor and target discrete elements are discretised into.
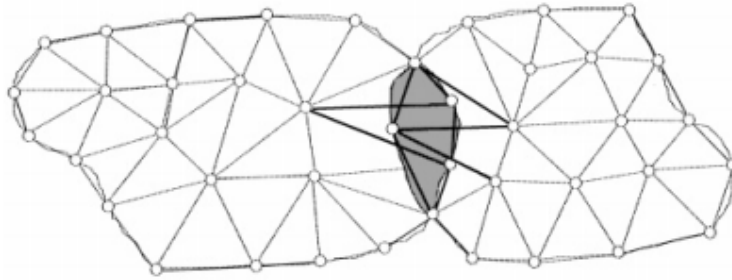

Figure 4 – Discretization of contactor and target into finite elements and integration over edges of overlapping elements. (Munjiza 2004)

3.3   Deformability

In FEMDEM, the deformability of individual discrete elements is captured by discretising into finite-elements. At each timestep, the Cauchy stress and Green-St.Venant strain fields are computed for each finite-element, which also describes fracture and fragmentation mechanics in large discontinuous problems. These constitutive laws apply only to visco-elastic materials. A concept of reference frames is used to describe the deformation of an individual discrete element. As deformation occurs, the deformed frame starts to differ from the initial frame, and is then related together by the deformation gradient **F** (Xiang et al. 2009).

The total Cauchy stress (true stress) for a visco-elastic material is given by:

$$\mathbf{T} = \frac{\mu}{J}(\mathbf{B} - \mathbf{I}) + \frac{\lambda}{J}(\ln J)\,\mathbf{I} + 2\eta\mathbf{D} \tag{6}$$

Where,
J is the determinant of the deformation gradient (the Jacobian determinant)
B is the Cauchy-Green tensor
D is the tensor rate of deformation obtained from the velocity gradient
η is the viscous damping coefficient
μ and λ are Lame constants defined by:

$$\mu = \frac{Y}{2(1+v)} \tag{7}$$
$$\lambda = \frac{v\,E}{(1+v)(1-2v)} \tag{8}$$

Where, E is Young's modulus and v is Poisson's ratio.

4   FEMDEM Numerical simulation setup

4.1   Simulation tools

Currently, there are 2 versions of *Y3D*. The first, is a complete FEMDEM code called *Y3D_D* (D for deformable) in which, individual discrete-elements are discretised into finite-elements, and deformation is incorporated by calculating the stresses of each finite element at each timestep. The other version is *Y3D_R* (R for rigid), which assumes a discrete body is rigid and skips the deformation calculations and runs significantly faster. **POSITIT** is a particle deposition program written by J Xiang which takes a grid input text file containing x y z coordinates, a mesh input file of the deposited particle, and Y3D input file. This is used in the following simulations to deposit particles with random orientations from the top of the container. A detailed section on the key **Y3D** simulation parameters is presented here, followed by the importance of mesh quality.

4.2   Critical timestep

There are different integration schemes available for evaluating the momentum conservation equations for each discrete element and node. In large FEMDEM simulations, implicit schemes become too computationally expensive to undertake, so explicit methods are more commonly employed. An explicit central difference time integration scheme is implemented in FEMDEM and this low order scheme reduces the number of operations executed because it doesn't require stiffness matrices.

Explicit integration schemes are conditionally stable, which means that the stability and accuracy of the scheme is dependent on the timestep used. The minimum timestep required to maintain stability is called the critical timestep. In FEMDEM, the critical timestep is proportional to the smallest finite element. This means that accuracy can be increased by reducing the meshing size, but a smaller timestep is required to maintain stability. Likewise, a larger timestep can be used if the meshing size is increased which allows larger timesteps to be used, so simulations can run faster. By assuming contact forces can be modeled as a simple 1D dashpot-spring system with no viscous damping, the critical timestep required, Δt_c can be approximated by Equation (9) (Guises et al. 2008):

$$\Delta t_c \leq 2\sqrt{\frac{m}{E}} \tag{9}$$

Where m is the mass of the smallest finite element, and E is the Young's modulus.

From this, it can be seen that the critical timestep is a function of the size of the smallest finite element, material density, and stiffness of the material. The penalty number selected will also affect the critical timestep. Note that this is an approximation for an undamped 1D system, which may not be suitable for 2D and 3D systems. Typically, the critical timestep calculated from Equation (9) is further divided 5 to 10 times to ensure stability and accuracy. Equation (10) is therefore used for calculating the critical timesteps used for the simulations in this paper. If there are large fluctuations in velocity values, then a smaller timestep needs to be used. This iterative process will ensure that the simulation uses less CPU time, without introducing instability and numerical simulation distortion.

$$\Delta t_c \leq \frac{1}{5}\sqrt{\frac{m}{E}} \qquad\qquad (10)$$

4.3   Penalty Number

The penalty parameter can be said to be a loose approximation of the surface roughness. If a small penalty number is used, then there will be a large overlap resulting in large errors in displacement. If an infinite penalty number is used, no penetration will occur. This often leads to problems in the temporal domain, so in practical applications, an overlap of contacting bodies is acceptable. The errors in displacement due to contact approximation can be reduced by selecting a suitable penalty number as a function of the Young's modulus, or by reducing the mesh size.

In packing density simulations using *Y3D_R*, the whole particle is treated as a rigid body with no deformation mechanics. The volume of overlap during penetration is small compared to the volume of the rigid body. As such, the penalty number used can be set to a value up to 10 times smaller than the Young's Modulus of a material. In the simulations performed, it was determined from trial and error that a penalty number of only 5 times smaller than the Young's Modulus was required to prevent excessive penetration.

However, in stress simulations using *Y3D_D*, the deformation of the discrete body is evaluated along with the stresses in the finite elements. The volume of the contacting overlaps can be quite a large fraction of a finite element, so to avoid errors in displacements due to excessive penetration of a body into another, the penalty number used needs to be about 10 times larger than the Young's Modulus of a material. In the simulations performed, it was determined from trial and error that a penalty number of only 2 times larger than the Young's Modulus was required to reduce the degree of penetration.

4.4   Material damping coefficient

The computational costs can become quite high when large numbers of interacting particles are modelled as fully deformable bodies (using *Y3D_D*). In gravity packing density simulations, the stresses within each do not become large enough to impact packing density results noticably. This is where *Y3D_R* can become very useful. By removing the internal deformation mechanics of discrete-elements, the total computation time can be reduced up to 5 times without much difference to the particle packing density.
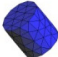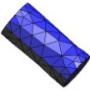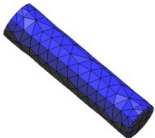
In a typical packing density simulation setup, particles are deposited into a container and the packing density is calculated only when the kinetic energy in the particles reduce to zero. The energy contained by a particle is dissipated through frictional contacts, Poissonal contraction and expansion behavior, and also through vibration resulting from stress waves propagating within deformable bodies. *Y3D_R* assumes these bodies are rigid, so the stresses are the same any point in a body. To account for the energy that would have been dissipated through vibration and deformation, a material damping coefficient is used in the rigid version to approximate the energy dissipation behavior in the material of a particle.

To determine a suitable material damping coefficient to use, gravity packing of particles into a container is simulated using *Y3D_D* with no material damping coefficient. Another set of simulations are done using *Y3D_R,* but with varying values of mass damping coefficients (i.e. 0.02, 0.04, 0.06, 0.08). The final packing density of *Y3D_R* simulations are calculated and compared to the packing density from the *Y3D_D* simulation. The most suitable material damping coefficient is the one which gives a packing density closest to the one obtained from *Y3D_D*.

In our investigations, a material damping coefficient of 0.05 was used for *Y3D_R* simulations. This value was determined by Xiang and Latham in their investigation of wooden cube packing in a wooden container. The applicability of this value of material damping coefficient to approximate *Y3D_D* behavior for different materials and geometries have not been investigated before, and is not verified in this paper due to time constraints. It is very possible that other material and geometry combinations require different material damping coefficients.

4.5   Mesh construction and the importance of mesh quality

As previously discussed, mesh quality is very important when it comes to FEMDEM simulations because of the discretization to finite elements. Finer mesh sizes represent contact behavior more accurately, but require a smaller timestep which increases the computational time. Coarser mesh sizes will allow larger timesteps to be used, and which also reduces computation time. The container and cylinder proppant geometries with aspect ratios of 0.5, 1.0, 2.0, 3.0, and 4.0 were generated using meshing software called *GiD 10.0.1* (Figure 5). When generating a mesh, few very fine elements are often found near the edges of a particle. A significantly smaller timestep is required just to maintain stability just for these few elements, which larger elements would not need. The simulation timestep can be optimized by coarsening these elements to allow a larger timestep to be used without decreasing the accuracy significantly. A guide to generating good meshes using *GiD 10.0.1* can be found in Appendix E.

Rod α = 0.5	**Rod α = 1.0**	**Rod α = 2.0**	**Rod α = 3.0**	**Rod α = 4.0**
138 elements	195 elements	392 elements	563 elements	762 elements
D = 0.01 m	D = 0.01 m	D = 0.01 m	D = 0.01 m	D = 0.01 m
L = 0.005 m	L = 0.01 m	L = 0.02 m	L = 0.03 m	L = 0.04 m
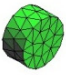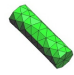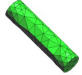
Rod α = 0.5 **Fixed volume**	**Rod α = 1.0** **Fixed volume**	**Rod α = 2.0** **Fixed volume**	**Rod α = 3.0** **Fixed volume**	**Rod α = 4.0** **Fixed volume**
127 elements	195 elements	187 elements	207 elements	345 elements
D = 0.0126 m	D = 0.0100 m	D = 0.0079 m	D = 0.0069 m	D = 0.0063 m
L = 0.0063 m	L = 0.0100 m	L = 0.0159 m	L = 0.0208 m	L = 0.0252 m

Figure 5 – A summary of the cylinder meshes created at 10:1 scale using GiD 10.0.1 (CIMNE 2011).

4.6   Material properties

The proppants deposited have been modeled with material properties of Bauxite (Table 1). This is a medium density ceramic with high compressive strength, which makes it well suited as a proppant material for withstanding high fracture closure stresses. It has also been widely used for spherical proppants. The material properties of Bauxite used in our simulations were an average of values reported by Pertti Auerkari (1996), Saint-Gobain Proppants (2011), and Carboceramics (2011).

Material property	**Value**		**Units**
Density (ρ)	3620		Kg/m^3
Young's modulus (*E*)	300		GPa
Penalty number	60 (Rigid)	600 (Deformable)	GPa
Poisson's ratio (*v*)	0.24		-
Friction coefficient (*μ*)	0.43		-
Material damping coefficient	0.05 (Rigid)	0 (Deformable)	-
Compression strength	86 (for 20-40 mesh)		MPa

Table 1 – Table summarising the Bauxite material and simulation parameters used.

5   Methodology

5.1   Simulation design for investigating packing porosity

In the first part of this work, the effect of cylindrical proppant with different aspect ratios (α = 0.5, 1.0, 2.0, 3.0, 4.0) and friction coefficients (μ = 0, 0.2, 0.4, 0.6, 0.8, 1.0) on the packing density was investigated in a 10:1 scale using **Y3D_R**. The influence of aspect ratio was investigated by 2 methods; Firstly, the lengths of the cylinders were varied with a fixed diameter (D = 0.01 m). From an engineering standpoint, the cylinders can be extruded using a standard process which will cheaper to produce. Secondly, from a theoretical standpoint, it is important to investigate aspect ratio effects independent of size. These particles were created to have the same volume as rods with α = 1.0, and scaled to reflect the correct aspect ratios. The friction coefficient simulations were performed only on rods with α = 1.0.

Cylindrical particles were deposited in arrays from a height of 15 cm, with a random orientation using **POSITIT**, into a container of internal dimensions 15 x 15 x 30 cm (Figure 6). The proppant particles settle under gravity to a height of 4 diameters. Ideally, more particles should be deposited to obtain a better representation of the packing porosity. This was not pursued in this investigation due to the computational time required. The simulation is stopped when the overall kinetic energy of the system stabilses to near zero, and the output mesh is then passed to a porosity calculation algorithm.
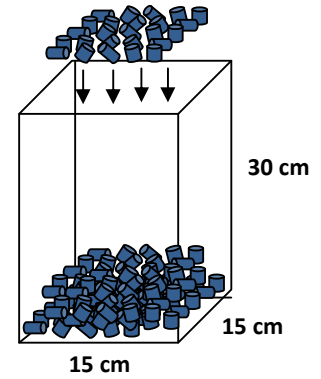

Figure 6 – Schematic of gravity deposition simulation setup

5.2   Simulation design for investigating stress distribution

In the second simulation case, the stress distributions within individual proppant particles were investigated in a 10:1 scale as a function of aspect ratio (α = 0.5, 1.0, 2.0, 3.0, 4.0). The cylindrical particles were deposited into a container of internal 15 x 5 x 10 cm using **POSITIT** with **Y3D_R**, until a packing height of about 4 diameters was obtained. After settling by gravity, a very high density slab with dimensions 14.95 x 4.95 x 2 cm was introduced to simulate fracture closure stresses acting on the proppant pack using **Y3D_D**. The plate was given an initial velocity of 1 m/s as a dead weight load control over the slab area to reduce the simulation times, and stress distributions at equilibrium should not be affected by this. (Figure 7)
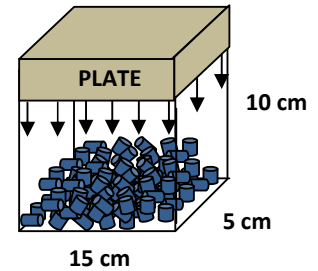
The sizing of the plate helps avoid stresses attributed to frictional contact with the container wall, and stresses arising from Poissonal contraction and expansions. By modifying the density of the plate, the simulated fracture closure stresses of 25 MPa can be adjusted to test different fracture closure stresses associated with rocks typically found at different depths. This method of stress loading was chosen because the stresses in the proppants increase gradually overtime, compared to when pressure or velocity conditions were applied. This avoids numerical simulation problems due to stress buffer size caused by rapid increase in stresses. At equilibrium, the stress distributions in proppants were analysed with a series of cross sections through the container.

Figure 7 – Schematic of stress loading simulation setup

5.3   Porosity calculation

Particles packing in a container are subject to wall effects which result from a tendency of particles to align thmeselves with the container wall. A combination of gravity and friction also contributes to the extent of the wall effect. Wall effects cause higher porosity to be observed in the near-wall region compared to the centre of the packing. To reduce this effect, a series of volumetric sampling windows were used. The dimensions of this sampling window were reduced by a distance of 0.5 diameters in all 6 dimensions in steps, until a reasonably consistent packing density was obtained. However, because the simulations were only packed up to 4D, only 1D could be excluded from the bottom end and the top of the packing (Figure 8).
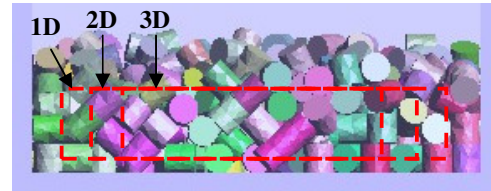

Figure 8 – Cross-sectional slice of packing bed. The volumetric domain used for porosity calculation is illustrated in red. 2D indicates that the volumetric domain was contracted by a distance of 2 diameters.

The porosity calculation program requires 3 input files. The first is a text file containing the number of random sample points, **N** and a user specified volumetric domain in which these points are generated. The other 2 input files are the **Y3D** and **ym** files corresponding to the final state of the system. **N** points are generated in this volumetric domain, and a voxel is created at each point. A voxel is assigned a value of '1' if it is located within a discrete element, or '0' is assigned, if it is void. The packing porosity is then obtained by computing the ratio of the number of voxels with a value of '0' by the number of voxels generated in this volumetric domain. The number of sample points generated is defined by the user, and the porosity calculation is run 3 times to obtain a range of porosity values. As with Monte Carlo sampling techniques, the porosity calculation becomes more accurate as sample points are increased. If there is a range of up to 1% between these values, the calculation is repeated with a larger number of sample points to obtain a consistent porosity value.

By this process, 50000 sample points was determined to be sufficient for this work. A plot of the number of sampling points against the accuracy of porosity calculation is shown in **Figure 9**.
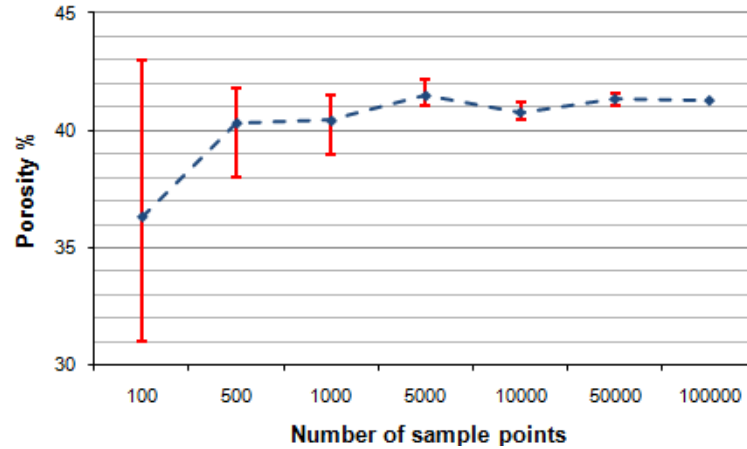

Figure 9 – Graph showing the accuracy of the porosity calculation programme as a function of the number of sample points used. 50000 sample points was deemed to be sufficient.

6   Simulation Results

We had initially set out to first, quantify the effects of aspect ratio and friction on the packing porosity of cylinders, and then investigate the stress distribution of different aspect ratio cylinders under stress loading of 25 MPa. Unfortunately, due to unforeseen length of simulation, only the investigations on cylinder aspect ratio, and friction could be completed within the timeframe of this study (Table 2). These simulations were done on a 10:1 scale to provide near proppant scale data on how different aspect ratio cylinders would resist fracture closure stresses while packing to higher porosity than spherical proppants. The total computational time is proportional to the size of the smallest element, and would run more quickly if a larger scale (e.g. 1000:1) was used for the simulations. This just highlights the need for Y3D to be parallelized before we can extend the capabilities to simulating large scale packing of particles.

In hindsight, our investigations could have been completed if it performed on 1000:1 scale for packing porosity simulations. The packing porosity is not expected to change significantly. For stress loading simulations on 1000:1 scale, stress scaling laws can be applied to recalculate the equivalent stresses in real life scale.

Investigation	Total runtime	Progress		Simulation Images
Aspect ratio (Fixed diameter)	44 days	Complete	**100%**	**Appendix B**
Friction coefficient	44 days	Complete	**100%**	**Omitted due to errors**
Aspect ratio (Fixed volume)	29 days	Still depositing	**60%**	**Appendix C**
Stress loading 25 MPa	18 days	Stress loading	**50%**	**Appendix D**

Table 2 –Status of our simulations at 10:1 scale.

6.1   Influence of wall effects

In cylinder packing, we observe three main factors which influence the packing porosity: orientation effects, volume exclusion effects, and cylinder aspect ratio. These exert their influence only in specific frictional and deposition conditions. When a particle is deposited, kinetic energy is dissipated to its surroundings as a combination of particle-particle contacts, particle-wall contacts, and gravitational effects. The particle continuously rearranges itself with nearby geometries to find a stable configuration until it loses all the energy. Energy loss is highest near the container walls due to face-wall frictional contacts. Under low friction setups ($\mu < 0.2$), very little energy is lost to particle contacts and more energy is available for rearrangement. As such, orientation effects tend to dominate in the near-wall region, and we observe high degree of ordering near the wall (also known as the wall effect) (Figure 10a). This can also occur when vibration is induced in packings to allow rearrangement. As friction increases, the packing structure near the wall become less ordered as more energy is required for rearrangement. (Figure 10b, 10c).
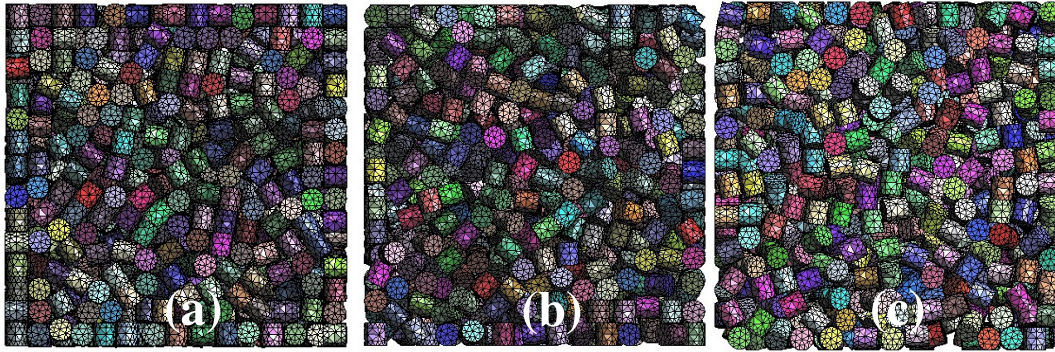

Figure 10 – View of packing structure at the base of container (looking upwards);
(a) High degree of ordering observed near the wall in equilateral cylinder packing with μ = 0;
(b) Lesser degree ordering observed near the wall in equilateral cylinder packing with μ = 0.4;
(c) Least degree ordering observed near the wall in equilateral cylinder packing with μ = 0.6.

In our loose packing simulations, we used a friction coefficient of 0.43 (Bauxite material) for the walls and particles to reduce the extent of ordered packing in the near-wall region. The porosity in the near-wall region is found to be higher (up to 10%) than in the centre of the pack (Figure 11). This indicates that the packings in near-wall regions were less ordered than in low friction cases, and wall effects penetrate less into the packing. As distance from the wall increases, the porosity is expected to stabilise but instead oscillations were observed even at a distance of 3D from the walls. This behavior can be attributed to calculation of porosity from a small volumetric domain of 9D x 9D x 9D, which is purely limited by our experimental setup. When plotting the aspect ratio versus packing porosity, we accounted for the fluctuating porosity calculations by averaging the porosities within the stable region (1D to 3D). Periodicity is observed for Rod 1, Rod 2 and Rod 3 as the porosity reaches a minimum at 0.5D and 1.5D. This periodicity decreases further away from the wall. This is explained by observing the ordering at the near-wall region (Roblee et al. 1958). Each particle that touches the wall is in a very ordered position, and the minimum porosity is observed at 0.5D from the wall because there is the highest concentration of particle centres in that area. Similarly, at 1 diameter from the wall, the porosity is at a maximum because there are void spaces in the interface between 2 layers of particles (Figure 12).
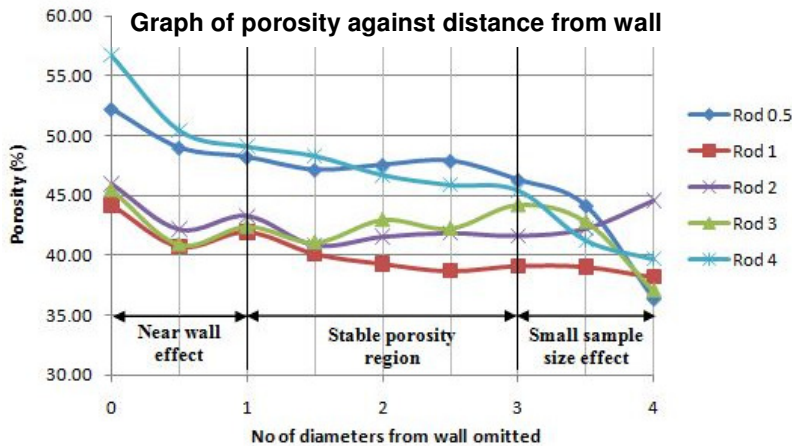

Figure 11 – Variation of porosity with the number of diameters from the wall omitted in porosity calculation volumetric domain.
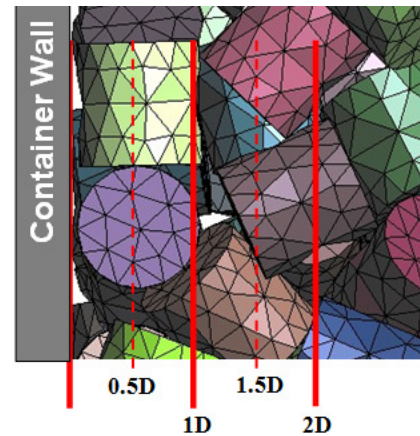

Figure 12 – Illustration of void interface between 2 ordered particles near the container wall.

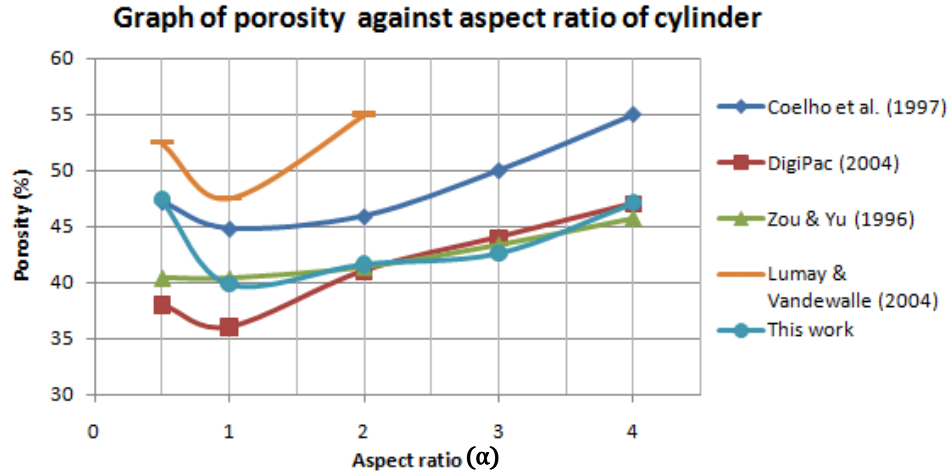## 6.2   Effect of aspect ratio on packing porosity

Figure 13 – Plot comparing the results of our investigation on cylinder aspect ratio vs. packing porosity with other studies found in literature. Friction coefficient of 0.43 was used in our simulations.

Our simulations results coincided well with Zou and Yu (1996) loose packing experiments, and DigiPac Monte Carlo geometric packing in a cylindrical column (Zhang 2006). They are presented in Figure 13. We observe a dip in packing porosity which is also documented in other studies when equilateral cylinders are used. Equilateral cylinders ($\alpha = 1$) exhibit the weakest orientation effects and form packs with more randomized orientations (Figure 14). This in theory should result in higher porosity packings due to less ordered structures, but it actually forms the densest pack of the cylinder aspect ratios investigated. This is because volume exclusion effects are small for equilateral cylinders (due to high symmetry) and pack like cubes. Packing porosity is also observed to increase when larger cylinder aspect ratios are used. Moderate-high friction setups reduce the extent of particle rearrangements and cause entanglements to form. The number of entanglements is related to the number of contacts-per-particle, and this increases with high aspect ratio cylinders. As a result, volume exclusion effects become more significant and porosity increases. Note that for cylinders with aspect ratio 0.5, the dip observed for aspect ratio 1.0 cylinder is about 7%. In the literature, this dip is reported to be within a range of 1% to 5%, and for this case, our results may be inaccurate due to a smaller sampling domain used compared to our other results. Refer to Appendix B for images.
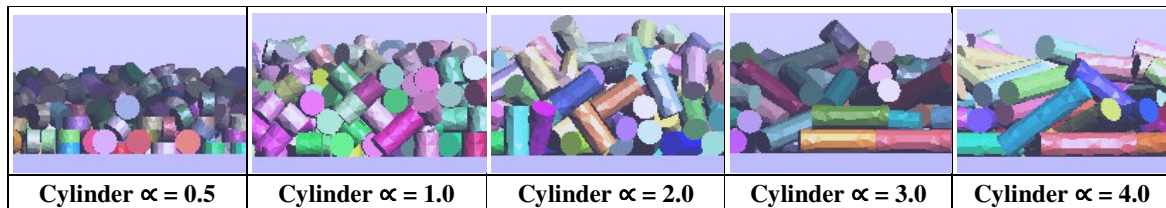

| Cylinder ∝ = 0.5 | Cylinder ∝ = 1.0 | Cylinder ∝ = 2.0 | Cylinder ∝ = 3.0 | Cylinder ∝ = 4.0 |

Figure 14 – Comparison of the packing structures from our investigation on cylinder aspect ratio (Fixed diameter)

6.3   Effect of size on packing porosity

The contact interaction algorithm in Y3D is based on a linear spring-dashpot model, which means that the contact force is a function of the mass of a particle. If two particles of different volumes made from the same material are deposited from the same height above a container, the larger particle would apply more energy. This means that a larger particle has more energy available for rearranging itself, unless the friction is high enough for size effects to be ignored. Visatemongkolchai (2010) observed in his tetrahedral packing simulations under different friction conditions, that size effects were insignificant for high friction coefficients (above 0.2). He also concluded that the size difference needs to be large enough to have an observable impact on packing porosity. In our simulations, cylinders with the aspect ratios 0.5, 2.0, 3.0, and 4.0 with the same volume as aspect ratio 1.0 cylinder (L = 0.01 m, D = 0.01 m) were packed to investigate aspect ratio effects independently of size. Unfortunately, because these particles were smaller, more of them needed to be deposited in the container to perform porosity calculations. This meant an even longer computational time was required, and we have not yet packed sufficient number of particles to analyse the results (currently 29 days runtime). These are still running on Imperial's CX1 HPC cluster, and analysis may be possible in the future. As such, our results on the effects of aspect ratio on packing porosity are not independent of size. The cylinder size effect is not expected to influence porosity results significantly. Refer to Appendix C for current progress.

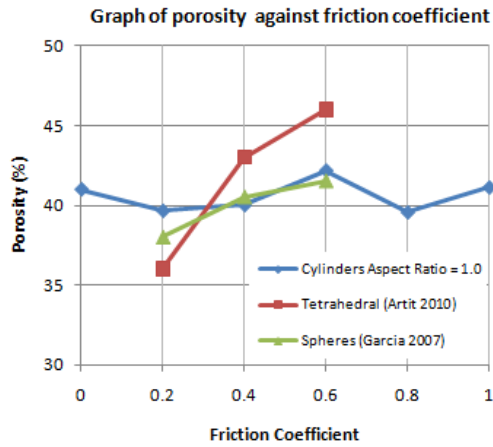## 6.4   Effect of friction factor on packing density

Figure 15 – Comparison of our cylinder with tetrahedral & sphere packing porosity under varying friction coefficients.
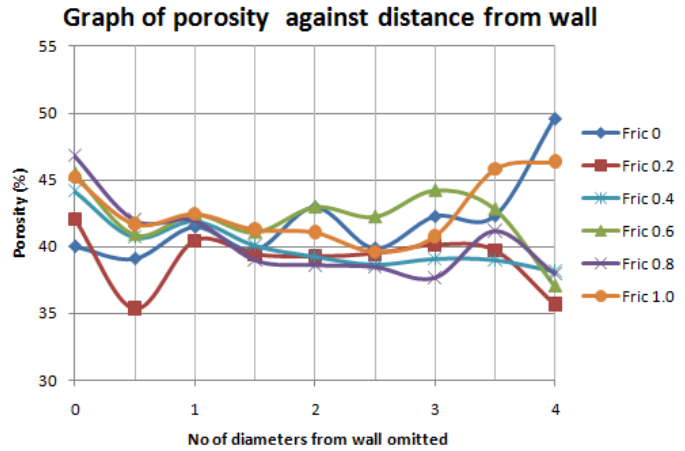
Figure 16 – Variation of porosity with the number of diameters from the wall omitted in porosity calculation volumetric domain.

As explained before in Section 6.1, particle rearrangement results in ordered packing structures where the porosity is low. When friction coefficient is increased, more energy is required for rearrangement and the packing structures are less ordered, resulting in higher porosity (Figure 16). Garcia's (2009) friction investigations on mono-sized spheres, and (Visatemongkolchai 2010)'s tetrahedral work, we expected to see a trend of porosity increasing as friction increases. This is not observed in our simulation results plotted on Figure 15, and on further inspection, we discover that the version of *Y3D_R* used for this set of simulations has a bug in the implementation of restart file (allows simulations to continue from previous saved timestep). The particle velocities after a restart file is used have a mismatch of up to 50%. This is significant, and would explain the apparent lack of trend observed in our porosity results for friction. In gravity packing simulations, settling velocity influences packing porosity results. High settling velocity means the particles contain more kinetic energy for significant rearrangement to occur, and generally results in lower porosity. Unfortunately, the nature of the velocity mismatch is quite random, and we cannot quantify the extent of this in our results. These investigations will be run 3 times with random particle orientations at a 1000:1 scale to investigate the variability in our results once this version of *Y3D_R* is fixed.

6.5   Effect of aspect ratio on stress distribution

During the undertaking of this research, simulation setups to investigate the effect of stress loading of cylinders with various aspect ratios were created and run using *Y3D_D* (describes deformations). This investigation is particularly interesting to industry because long aspect ratio cylindrical proppants will be subject to compression, friction, and also 3-point-bending modes which will induce tensile and compressive stresses that will significantly reduce the strength of ceramic cylinders This deformation is described well by *Y3D_D*. (Figure 17). Also due to computing and time limitations, the investigations on this have not yet been concluded, and further work is required. This investigation will benefit greatly from the parallelisation of *Y3D_D* because the timestep required for stable simulation of 10:1 scale particles under 25 MPa stress is in the magnitude of 2.5×10^{-10} seconds. Shorter simulation times would mean we will be able to numerically simulate particle scale proppants in the future. Another way to accomplish this is to model the setup with a larger scale of 1000:1. From our testing, we have observed that simulations run at 1000:1 scale decreases the total computation time up to 8 times compared to at 10:1 scale. Stress simulations at 1000:1 scale would require in-depth understanding of stress scaling laws to convert results obtained to an equivalent stress under real life proppant scale for percentage breakage analysis. Refer to Appendix D for current progress.
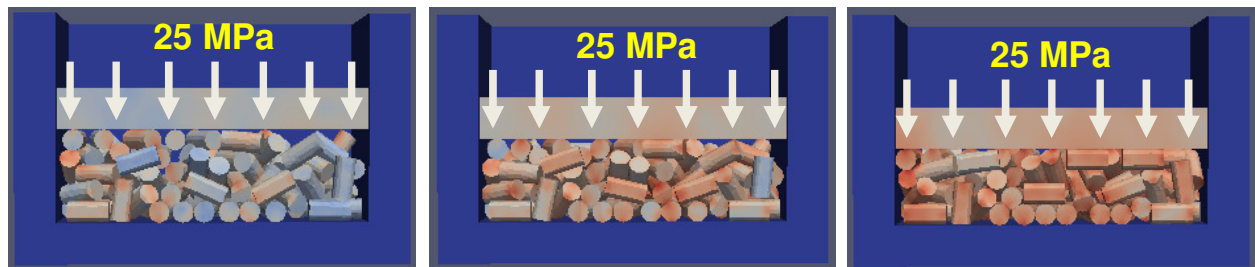

Figure 17 – Stress loading simulation of cylinders with aspect ratio 2.0. Red represent high stresses in magnitude of 10^{10} Pa. A logarithmic scale is used here to show stresses propagating through the pack.

7   Conclusions

In this paper, we described a framework to investigate the effect of cylinder aspect ratio and friction on the packing porosity, and also the internal stresses resulting from stress loading of cylinder geometries using 3D FEMDEM. These investigations were performed at a 10:1 scale because of industry interest in particle scale simulations. We have also performed alternative simulations on a 1000:1 scale for investigating the total computation time required. Our main conclusions from this research are as follows:

1) Parallelisation needs to be implemented in **Y3D_R** to simulate suffient numbers of particles at 10:1 within a reasonable timescale.
2) Problem in **Y3D_R** restart subroutine implementation causes velocity mismatches which invalidate our friction investigations.
3) Simulations of packing porosity of different aspect ratio cylinders using **Y3D_R** agreed well with experiments and simulations of cylinder packing.
4) **Y3D_R** can generate packing structures which are qualitatively similar to experimental results on cylinders in literature. Periodicity in the near-wall region due to local particle ordering is also observed.
5) Packing simulations with 648 particles at 10:1 scale took 8 times longer to complete compared to 1000:1 scale.
6) Further work on friction and stress investigations at 1000:1 scale with current **Y3D** code would have been been more appropriate for our timeframe.
7) Further simulations should be performed to test the variability of porosity results, as we know packing porosity is very sensitive to initial deposition conditions. (Latham and Munjiza 2004)
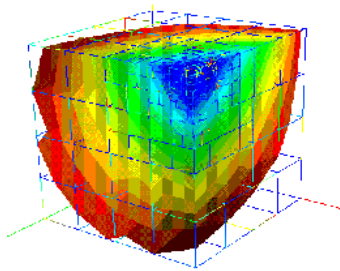
8   Recommendation of future work

Figure 18 – 3D representation of a discretised domain for 64-core parallel computation. (M. Griebel 1998)

8.1   Parallelisation

From our investigations of the effect of cylinder aspect ratio on the packing porosity, the average runtime for these simulations with **Y3D_R** were found to be atleast 40 days for 648 particles with a timestep of 1×10^{-7} seconds required to maintain numerical stability. This timestep is a function of the volume of the smallest discrete element, and at 10:1 scale, this is very small. Additionally, the number of particles and the mesh sizes of the particles used also increase the computational time when more particles are in contact.

To tackle larger problems at a scale of 10:1, *Y3D* needs to be parallelized so that the computational space is discretised into smaller domains which can employ more CPU cores for computation (Figure 18). This will significantly reduce the total computational time of 3D FEMDEM, and extend the capabilities of this code for tackling larger computational problems involving smaller scales and more particles.

8.2   Flow simulations to investigate effective permeability of packed beds of cylinders

The key issue the industry is interested in is the modeling of flow through cylinder packed beds. Experiments have been performed on flow through sphere packed beds (Sharma et al. 2001) (Garcia 2009), but none on cylinders. It will be beneficial to investigate how the effective permeability of cylinder packs is influenced by cylinder aspect ratios. This can be done by adapting the meshes of gravity packed cylinder beds generated from our research for flow simulations using our fluid code *FLUIDITY*, as done by Garcia et al. (2009) in Figure 19.

With further development, the coupling of *FLUIDITY* with **3D FEMDEM** can model the migration path of fine particles suspended in a fluid through a packed bed. The deposition mechanism could then include sedimentation and buoyancy effects instead of gravity deposition, and allow us to simulate the clogging of proppant beds in propped fractures with fine particles. This has important applications for understanding the effect of fines in hydraulic fracturing on fracture conductivity, as well as the efficiency of water filtration systems.
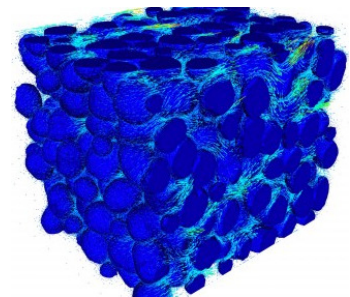

Figure 19 – Flow simulation through void space mesh of a packed bed using FLUIDITY. (Garcia 2009)

8.3   Stress loading simulations of packed beds of cylinders with different aspect ratios

We have documented our attempts to investigate this at a scale 10:1 in Section 6.5, but were unable to conclude our analysis due to length of simulations. Future work is recommended at a larger scale of 1000:1. From our testing, we have observed that shorter computation times of up to 8 fold (compared to 10:1 scale simulations) for gravity packing simulations using **Y3D_R**, and have reasonable assumption that this will also be observed in **Y3D_D**. Stress simulations at 1000:1 scale would require in-depth understanding of stress scaling laws to convert results obtained to an equivalent stress under real life proppant scale for percentage breakage analysis. The models we have created at 10:1 scale can also be modified to perform stress loadings of different magnitudes (i.e. 12 MPa, 50 MPa, 75 MPa), on different particle geometries (Figure 20).

Refer to Appendix D for current progress. For a guide on creating these stress loading simulations, refer to Appendix E.
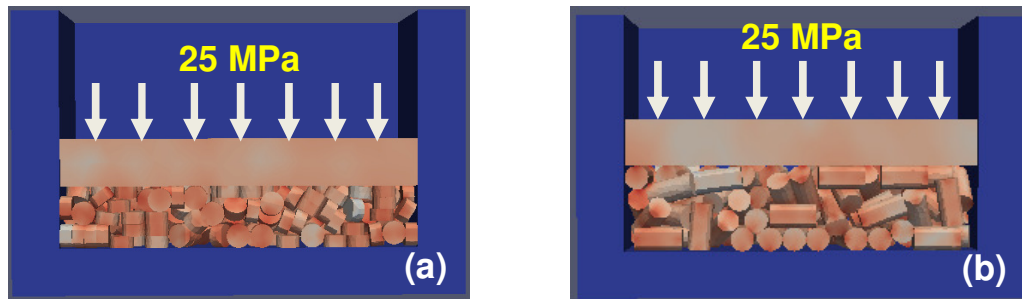

Figure 20 – Stress loading simulation of cylinders with (a) aspect ratio = 0.5, and (b) aspect ratio = 2.0 using Y3D_D. A logarithmic scale is used here to show stresses propagating through the pack.

8.4   Coupling of 3D FEMDEM with Mohr-Coulomb fracture model

By coupling 3D FEMDEM with a Mohr-Coulomb criterion fracture model, the effects of fines production due to crushed proppants under high stresses can be investigated. This will also be an interesting tool in the development of catalytic pellet reactors which require large surface area to volume ratios with the low pellet breakage.

9   Nomenclature

α	=	aspect ratio, fraction	MPa	=	mega (1e6) Pascal, m/Lt^2
D	=	diameter, L, m	μ	=	friction coefficient, dimensionless
E	=	Young's modulus, m/Lt^2, GPa	ρ	=	density, m/L^3, kg/m^3
GPa	=	giga (1e9) Pascal, m/Lt^2	Δt_c	=	Critical time-step, t, seconds
L	=	length, L, m	ν	=	Poisson's ratio, fraction
m	=	Mass, m, kg			

10   References

Prats. "Effect of Vertical Fractures on Reservoir Behavior - Incompressible Fluid Case." *SPE 1575-G, Journal Volume 1, Number 2*, **1961**: 105-118.

API RP 19C. "Measurement of Proppants Used in Hydraulic Fracturing and Gravel-packing Operations." *API*, 2008.

Visatemongkolchai A. "Modelling porosity of sand deposits consisting of angular grains." *Imperial College London MSc Petroleum Engineering*, 2010.

Benyahia and O'Neil. "Enhanced Voidage Correlations for Packed Beds of Various Particle Shapes and Sizes." *Particulate Science and Technology* Vol. **23**, Iss. 2, 2005: 169-177.

Benyahia, F. "On the global and local structural properties of packed beds of non-equilateral cylindrical particles*." Particulate Science and Technology* **14** (3), 1996: 221-237.

Carboceramics. CARBO HSP. 2011. http://www.carboceramics.com/CARBO-HSP/ (accessed 8 29, 2011).

Carman, P.C. "Fluid flow through granular beds." *Transactions, Institution of Chemical Engineers, London*, 1937: **15**:150-166.

CIMNE. 2011. http://gid.cimne.upc.es/ (accessed 8 29, 2011).

Coelho et al. "Geometrical and transport properties of random packing of spheres and aspherical particles." *Phys. Rev. E*, **55** (2), 1997: 1959-1978.

Cundall and Strack. "A discrete numerical model for granular assemblies." *Geotechnique*, **29**, 1979: 47–65.

Dixon, A.G. "Correlations for wall and particle shape effects on fixed bed bulk voidage." *Canadian Journal of Chemical Engineering* **66**, 1988: 705-708.

Ergun, *S. Chem. Process Eng. London* **48**, 1952: 89 .

Foumeny and Roshani. "Mean voidage of packed beds of cylindrical particles." *Chemical Engineering Science* **46** (9), 1991: 2363-2364.

Garcia et al. "Numerical study of the effects of particle shape and polydispersity on permeability." *Physics Review E*, Vol **80**, 2009: doi/10.1103/PhysRevE.80.021304.

Garcia. "Numerical modelling of the microstructure and permeability of granular materials." *Imperial College London PhD Thesis*, 2009.

Guises et al. "Granular packing: numerical simulation and the characterisation of the effect of particle shape." *Imperial College London PhD*, 2008.

Jiansheng Xiang, Antonio Munjiza, John-Paul Latham, Romain Guises. "On the validation of DEM and FEM/DEM models in 2D and 3D." *Engineering Computations: Int J for Computer-Aided Engineering*, Vol. **26**, No. 6, 2009: 673-687.

Kozeny, J. "Ueber kapillare Leitung des Wassers im Boden." Sitzungsber Akad. Wiss., Wien, **136**(2a): 271-306 (1927).

Latham and Munjiza. "The modelling of particle systems with real shapes." *Phil. Trans. R. Soc. Lond. A* vol. **362** no. 1822, 2004.

Lumay and Vandewalle. "Compaction of anisotropic granular materials: experiments and simulations." *Phys. Rev. E* **70**, 051314, 2004.

M. Griebel, G. Zumbusch, J. Mandel, C. Farhat, X.-C. Cai. "Hash-Storage Techniques for Adaptive Multilevel Solvers and their Domain Decomposition Parallelization." *Proceedings of Domain Decomposition Methods 10, Contemporary Mathematics* **218**, AMS, 1998: 279-286.

Montillet and Le Coq. "Characteristics of fixed beds packed with anisotropic particles-Use of image analysis." *Powder Technology* **121**, 2001: 138-148.

Munjiza and Andrews. "NBS contact detection algorithm for bodies of similar size." *International Journal for Numerical Methods in Engineering.* **43**, 1998: 131-149.

Munjiza and Andrews. "Penalty function method for combined finite-discrete element systems comprising large number of separate bodies." *Int. J. Numer. Meth. Engng* **49**, 2000: 1377-1396.

Munjiza. "The Combined Finite-Discrete Element Method". *Wiley*, 2004.

Munjiza, A. "PhD Swansea University." 1990.

Nandakumar, K., Shu, Y. and Chuang, K. T. "Predicting geometrical properties of random packed beds from computer simulation." 2286–2297, 1999: 2286–2297.

Nardin et al. "Contribution a l'Etude des Empilements au Hasard de Fibres etou de Particules Spheriques." Powder Technology 44, 1985: 131-140.

Neto, E. A. S., Pires, F. M. A. and Owen, D. R. J. "F-bar-based linear triangles and tetrahedra for finite strain analysis of nearly incompressible solids. Part I: formulation and benchmarking. ." *International Journal for Numerical Methods in Engineering*, **62**, 2005: 353–383.

Pertti Auerkari. "Mechanical and physical properties of engineering alumina ceramics." *VTT Tiedotteita - Meddelanden - Research Notes* **1792**, 1996.

R. Caulkin, X. Jia, C. Xu, M. Fairweather, R. A. Williams, H. Stitt, M. Nijemeisland, S. Aferka, M. Crine, A. Leonard, D. Toye, and P. Marchot. "Simulations of Structures in Packed Columns and Validation by X-ray Tomography." *Ind. Eng. Chem. Res.* **48**, 2009: 202-213.

Roblee et al. "Radial porosity variations in packed beds." *A.I.Ch.E. Journal* **4**, 1958: 460-464.

Saint-Gobain Proppants. "Ultraprop Sintered Bauxite." Saint-Gobain Proppants - Ultraprop Sintered Bauxite. 2011. http://www.oilandgas.saint-gobain.com/uploadedFiles/SGoilandgas/Documents/Proppants/Ultraprop-SB.pdf (accessed 8 29, 2011).

Sharma et al. "Determination of bed voidage using water substitution and 3D magnetic resonance imaging, bed density and pressure drop in packed bed reactors." *Chemical Engineering Science* **56** (2), 2001: 587-595.

Sherwood, J D. "Packing of spheroids in three-dimensional space by random sequential addition." *J. Phys. A: Math. Gen.* **30**, 1997: L839–L843.

SPE 135360. "Changing the Shape of Fracturing: New Proppant Improves Fracture Conductivity." *SPE Annual Technical Conference and Exhibition*, **19-22 September 2010**, *Florence, Italy.*

SPE 143426. "Optimizing Production of Tight Gas Wells by Revolutionizing Hydraulic Fracturing." *SPE Project and Facilities Challenges Conference at METS,* **13-16 February 2011***, Doha, Qatar.*

Stoyan. "Mathematical model and solution method of optimization problem of placement of rectangles and circles taking into account special constraints." *International Transactions in Operational Research*, vol. **5**, no. 1, 1998: 45–57.

Stoyan. "Simulation and Statistical Analysis of Random Packings of Ellipsoids." *Part. Syst. Charact.* **23**, 2006: 388–398.

Villarruel et al. "Compaction of rods: relaxation and ordering in vibrated, anisotropic granular material." *Physical Review E* **61** (6), 2000: 6914-6921.

Visscher and Bolsterli. "Random Packing of Equal and Unequal Spheres in Two and Three Dimensions." *Nature* **239**, 1972: 504-507.

Vold, Marjorie J. "Computer simulation of floc formation in a colloidal suspension." *Journal of Colloid Science*, Volume **18**, Issue 7, 1963: 684-695.

Vold, Marjorie J. "Sediment Volume and Structure in Dispersions of Anisometric Particles." *J. Phys. Chem.* **63** (10), 1959: 1608–1612.

Vold, Marjorie J. "The sediment volume in dilute dispersions of spherical particles." *J. Phys. Chem.* **64** (11), 1960: 1616–1619.

Wenli Zhang, Karsten E. Thompson, Allen H. Reed, Liese Beenken. "Relationship between packing structure and porosity in fixed beds of equilateral cylindrical particles." *Chemical Engineering Science*, Volume **61**, Issue 24, 2006: Pages 8060-8074.

Williams and Philipse. "Random packings of spheres and spherocylinders simulated by mechanical contraction." *Physical Review. E*, Statistical, Nonlinear, and Soft Matter Physics **67**(5 Pt 1), 2003.

Wouterse et al. "Effect of particle shape on the density and microstructure of random packings." *J. Phys. : Condens. Matter* **19** 406215, 2007.

Xiang et al. "Finite strain, finite rotation quadratic tetrahedral element for the combined finite-discrete element method." *International Journal for Numerical Methods in Engineering.* **79**(8), 2009: 946-978.

Zhang, Wen li. "Experimental and computational analysis of random cylinder packings with applications." *PhD Louisiana State University*, 2006.

Zou and Yu. "Evaluation of the packing characteristics of mono-sized non-spherical particles." *Powder Technol.*, **88**, 1996: 71-79.